Learning Topology Uniformed Face Mesh by Volume Rendering for Multi-view Reconstruction

Yating Wang[1], Ran Yi[1], Ke Fan[1], Jinkun Hao[1], Jiangbo Lu[2], and Lizhuang Ma[1]

[1] Shanghai JiaoTong University, Shanghai, China
[2] SmartMore Corporation

Abstract. Face meshes in consistent topology serve as the foundation for many face-related applications, such as 3DMM constrained face reconstruction and expression retargeting. Traditional methods commonly acquire topology uniformed face meshes by two separate steps: multi-view stereo (MVS) to reconstruct shapes followed by non-rigid registration to align topology, but struggles with handling noise and non-lambertian surfaces. Recently neural volume rendering techniques have been rapidly evolved and shown great advantages in 3D reconstruction or novel view synthesis. Our goal is to leverage the superiority of neural volume rendering into multi-view reconstruction of face mesh with consistent topology. We propose a mesh volume rendering method that enables directly optimizing mesh geometry while preserving topology, and learning implicit features to model complex facial appearance from multi-view images. The key innovation lies in spreading sparse mesh features into the surrounding space to simulate radiance field required for volume rendering, which facilitates backpropagation of gradients from images to mesh geometry and implicit appearance features. Our proposed feature spreading module exhibits deformation invariance, enabling photorealistic rendering seamlessly after mesh editing. We conduct experiments on multi-view face image dataset to evaluate the reconstruction and implement an application for photorealistic rendering of animated face mesh.

Keywords: Multi-View Face Reconstruction · Mesh Topology · Neural Volume Rendering

1 Introduction

The uniformed topology face mesh dataset serves as the cornerstone for many face-related applications. It inherently encodes dense vertex correspondence among faces with varying shapes and expressions, greatly simplifying human faces interpolation, analysis, and manipulation. For example, the classical statistical face model 3DMM [3] is derived from the uniformed topology face mesh dataset, enabling applications such as monocular face reconstruction and animatable avatars. However, obtaining a topology uniformed face mesh is not straightforward. A classic procedure involves initially reconstructing scans using multi-view
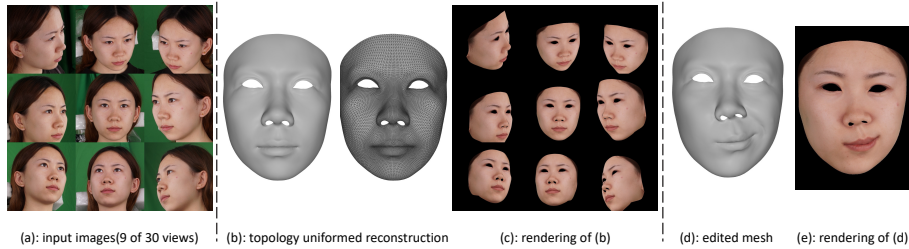
(a): input images(9 of 30 views) ┊ (b): topology uniformed reconstruction   (c): rendering of (b)   ┊   (d): edited mesh   (e): rendering of (d)

Fig. 1: We propose a method that simulates the radiance field using meshes, enabling direct reconstruction of topologically uniformed face meshes from multi-view images through volume rendering. After face animation, the rendering quality remains consistent with the original images. (a) input multi-view images; (b) reconstructed topologically uniformed mesh; (c) rendering of reconstruction; (d) animated face and (e) rendering of animated face mesh.

stereo algorithms and subsequently deforming a mesh template with predefined topology to tightly match the scans using non-rigid registration algorithms. Commonly used statistical face models, such as [3, 19, 33, 48], are derived based on this procedure.

Nevertheless, this procedure may encounter a bunch of issues. Firstly, scans often contain irregular noise, requiring manual cleaning-up and hyperparameter adjustment to ensure convergence during the registration step. The errors of scans are carried over into the registration results, leading to error accumulation. Besides, traditional MVS software relies on image feature extraction and matching, making it challenging to handle surfaces with complex material properties, as commonly found in human faces. Currently some neural network methods can directly predict uniformed topology meshes from multi-view face images, but they rely on scans [4] or registrations [20, 21] output by the mentioned procedure to serve as ground truth supervision.

In recent years, there has been a continuous integration of deep learning with traditional 3D computer vision and graphics algorithms. Methods based on volume rendering and neural implicit 3D representations, *e.g.,* NeRF [29], NeuS [38] and others [8, 24, 25, 42], leverage the powerful fitting capabilities of neural networks to model geometry, anisotropic appearance and lighting. The well-behaved differentiability of volume rendering allows gradients to be computed throughout space, and enables efficient back-propagation of loss functions from images to directly optimize network parameters. These approaches have achieved remarkable results in tasks such as 3D reconstruction, novel view synthesis, and realistic rendering, gaining widespread attention. Our goal is to combine the end-to-end gradient backpropagation of neural volume rendering with the ability to handle complex appearance and lighting, achieving a method to reconstruct uniformed topology meshes from multi-view images as an alternative to the MVS+registration procedure.

We propose a new mesh volume rendering mechanism to enable topology-consistent reconstruction. The main challenge in mesh-based volume rendering is that classic volume rendering methods operate on density and color fields, which assign values to every point in the space. However, mesh only describes the surface of objects, so it only has values in a small region within the space. The core of our method is how to spread sparse surface features into the surrounding space, thereby simulating a density and radiance field. Firstly we compute the nearest distance from sampling points to the mesh and employ the method similar to [24, 25, 28, 38] to convert distance into volume rendering density. Secondly, we propose a learnable feature spreading module, which spreads surface features into surrounding space to simulate a radiance field. Utilizing density and radiance field simulation, we employ volume rendering to backpropagate loss from images, in order to optimize the vertex positions of a template mesh, implicit features defined in UV space, and parameters of the feature spreading module. Additionally, the simulated radiance field is encoded in relative coordinate system of the mesh, thus when the mesh moves, the radiance field moves relatively. Leveraging this property, we can edit face mesh using deformation algorithms such as blendshapes while maintaining the same rendering quality. The reconstructed geometry, textures, and feature spreading modules together can function as animatable face avatars.

Contributions of this paper can be summarized as:

- We propose a novel schema for neural volume rendering on triangle meshes, enabling direct reconstruction of topology consistent face mesh from multi-view images.
- We propose a deformation-invariant features spreading module to spread sparse implicit features defined on mesh surface into surrounding space and simulate a continuous radiance field, which enables photorealistic rendering after face animation.
- Qualitative and quantitative experiments are conducted to demonstrate the effectiveness of the proposed method. And the corresponding code will be publicly accessible.

2   Related works

2.1   Multi-view face reconstruction

Typically, high quality multi-view uniformed topology face reconstruction involves two steps: multi-view stereo geometry reconstruction and non-rigid topology registration. Multi-view face images can be captured with passive multiple camera system [2] or active photometric stereo systems [11, 27]. Subsequently, 3D reconstruction algorithms based on image feature matching and multi-view geometry are used to recover scans from the images. Some commercial softwares provide this functionality, such as Colmap and Metashape. And then non-rigid registration algorithms are used to deform a template mesh to fit the captured geometry for topology aligning mostly regularized by statistics face model [19],

or jointly optimize correspondence across an entire dataset in a groupwise manner [5, 53]. Scans often have irregular noise, necessitating manual cleaning-up or hyperparameter adjustment for convergence of registration. And errors in the raw scan may propagate into the registration results. [9] directly recovers uniform topology geometry from images without the need for acquiring scans. However, this method is based on optical flow, making it sensitive to environment lighting and self-occlusion. There are some learning based topologically uniformed face mesh reconstruction methods. [4, 20, 21] learn to regress topology uniformed face mesh from multi-view images, but require large amount of ground truth scans or registered meshes for training, which requires much computation resources. [1, 39] use 3DMM [3] as shape prior, limiting the method usable only on the topology where 3DMM is based. Switching to different topology entails much additional efforts. Our method, on the other hand, only annotates sparse landmark indices for each predefined topology, making it relatively easy to transition to a different topology. Additionally, recent works like [6, 10, 12, 14, 35, 55] focus on reconstructing drivable neural avatars based on implicit representations from monocular face videos. A large portion of these methods are conditioned on 3DMM coefficients or bound to uniformed topology meshes.

2.2   Neural Rendering Mesh Reconstruction

Existing multi-view reconstruction softwares, such as COLMAP, relies on image feature extraction and matching which can produce precise results but struggles with noise and non-Lambertian surfaces. Recently, neural rendering methods make significant advancements in mesh 3D reconstruction. Some works [7, 15, 17, 22, 23, 26, 31, 43] transform discrete rendering (rasterization or ray tracing) into a continuous and differentiable form, enabling mesh reconstruction by inverse rendering. Recently NeRF [29] achieves remarkable results in novel view synthesis tasks, utilizing volume rendering to efficiently backpropagate gradients, which is capable of handling intricate occlusion and modeling complex interactions between illumination and surface materials. Thus differentiable volume rendering has garnered significant attention. Explicit 3D meshes can be extracted from NeRF [29] but with much noise. Methods like [24, 25, 32, 38, 49], replace density field by distance field for smooth and accurate surfaces reconstruction. After acquiring implicit distance field, marching cubes or [37] are applied for explicit mesh extraction. Nevertheless, topology of meshes obtained by the above methods is not fixed and the topological quality may be poor, thus additional registration step is required for topology consistency.

2.3   Mesh in Neural Volume Rendering

There are many methods attempting to incorporate meshes into volume rendering, primarily for NeRF [29] real-time rendering or editability. [8] combines traditional graphics rasterization pipelines with neural rendering attributes, achieving fast NeRF rendering. [37, 50] extract high quality meshes in free topology from implicit representation thus enabling mesh physics simulation and rasterization.
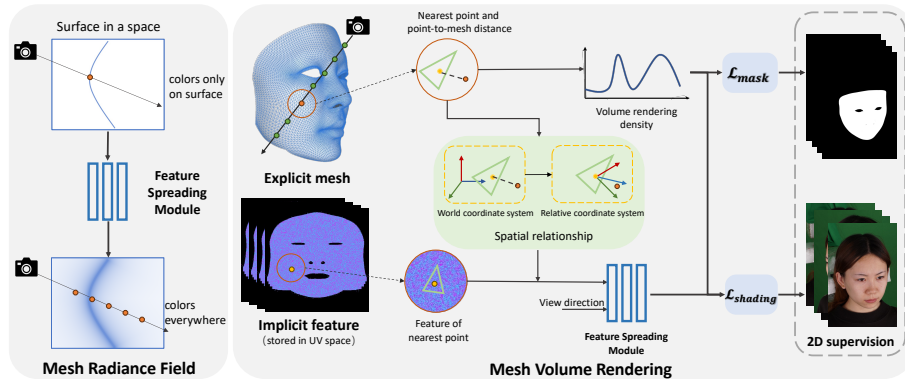
Fig. 2: The pipeline of our proposed approach. We propose a mesh volume rendering mechanism which transforms point-to-mesh distance into density, and a learnable mesh features spreading module, which spreads sparse features defined on mesh surface into surrounding space to simulate a continuous radiance field. Our method can generate high-quality images from mesh by volume rendering, thus enabling loss backpropagation from image to mesh parameters (vertice position and implicit features defined in UV space).

Some works [13, 42] leverage hybrid representation of mesh and implicit field based on the observation that solid objects are better described using meshes that can be quickly rendered, while implicit representation are more suitable for objects challenging to model geometrically such as hair or grass. [44,45,47,51,52] bind NeRF to the mesh, and when editing mesh shape, the implicit field changes accordingly. Similarly, [34,46] encapsulate NeRF within a cage represented by a mesh, using the deformation of the enclosing mesh to drive the internal motion of NeRF. These methods do not focus on reconstruction and maintaining topological consistency, and all require first reconstructing implicit 3D shape before extracting explicit meshes. In contrast, our method directly reconstructs shapes from multi-view images while preserving topological consistency.

3   Method

Given multi-view images with known camera parameters and a face mesh template predefined by artists as inputs, our proposed method directly optimizes mesh geometry while maintaining topology consistency, and learns implicit texture features. Our pipeline is shown in Fig2. First, we propose a new mesh volume rendering mechanism with mesh features spreading module, which propagates features defined on the mesh surface into the surrounding space, allowing the mesh to simulate a radiance field, based on which volume rendering can backward loss from images to mesh parameters. 1) In mesh volume rendering, for each sampled point along a ray, we search for the nearest point on the mesh, and the distance between these two points is converted into density. 2) mesh

feature spreading: Features of nearest point, relative spatial vector, and viewing direction are then fed into learnable features spreading MLP to obtain color of sampled points.

Based on this mesh volume rendering mechanism, we optimize the vertices positions $V \in \mathbf{R}^{n_v \times 3}$ of a template mesh whose topology $F \in \mathbf{Z}+^{n_t \times 3}$ is predefined by artists and fixed during optimization, to approximate multi-view images $\{I_i\}_{i=1}^{M}$ in M views with known camera parameters (denoted by $\{K_i, R_i, t_i\}_{i=1}^{M}$) for different identities and expressions. For appearance modeling, we learn an implicit appearance feature $A \in \mathbf{R}^{n_a \times n_a \times n_f}$ defined in UV space (n_f, n_a denote feature dimension and size of the square texture feature), and a MLP-based features spreading module $\mathcal{F}_d$ to decode implicit features and spread color into surrounding space.

This section will be arranged as following: Section 3.1 reviews SDF volume rendering method proposed in NeuS [38]. Section 3.2 provides an overview of our proposed mesh volume rendering process and formulas, explaining the transformation from point-to-mesh distance to density for volume rendering. The mapping from implicit mesh texture features to radiance field will be introduced in Section 3.3. In Section 3.4, we present the loss functions, training process and strategies.

3.1   Preliminaries

In this section, we review the volume rendering process proposed in NeuS [38]. Considering a ray $\mathbf{r}$ emanating from the camera center $\mathbf{o} \in \mathbf{R}^3$ in direction $\mathbf{v} \in \mathbf{R}^3(||\mathbf{v}|| = 1)$, which is parameterized by $\{\mathbf{r}(t) = \mathbf{o} + t\mathbf{v} | t \geq 0\}$, the accumulated color $\hat{C}$ of the pixel corresponding to the ray $\mathbf{r}$ is calculated by:

$$\hat{C}(\mathbf{r}) = \sum_{k=1}^{N} T_k \alpha_k \mathbf{c}_k, \quad T_k = \prod_{k'=1}^{k-1} (1 - \alpha_k), \tag{1}$$

where N denotes the sampling points number along the ray $\mathbf{r}$. T_k is the accumulated transmittance, and α_k is the weight of the k-th sample point.

Since in NeuS the geometry of the scene is represented by signed distance field (SDF) instead of volume density, a mapping function from SDF values to the weight α_k is designed. It has been demonstrated that the density function along a ray needs to be monotonically increasing before and after traversing the surface. This ensures unbiased weighting in volume rendering and awareness of occlusion. The volume rendering density α proposed by NeuS [38] is formulated as:

$$\alpha_k = max\left(\frac{\Phi_s(s_k) - \Phi_s(s_{k+1})}{\Phi_s(s_k)}, 0\right) \tag{2}$$

where Φ_s is the cumulative distribution of logistic density distribution, and s_k is the SDF value of the k-th sample point.

The SDF representation used in NeuS assumes that the object to be reconstructed is watertight, but cannot handle reconstruction of non-closed shapes. To reconstruct general objects, some methods [24,25,28] leverage neural implicit Unsigned Distance Field (UDF) instead of SDF.

3.2   Mesh Volume Rendering

In this section, we introduce how to perform volume rendering on mesh. We develop a mesh volume rendering scheme inspired by NeuS, but make adaptations tailored for mesh: a density calculation method based on the distance from point to mesh, a normal approximation method for sampling points not on the mesh surface, and a sampling method with reduced sample points.

Mesh Density. Firstly, we transform point-to-mesh distance to density using the similar algorithm proposed in NeuS [38]. Signed Distance Field (SDF) is a function that represents the signed minimal distance from a point in space to surface. Given a mesh, we compute the distance field by searching the nearest point on mesh surface. For each sample point $\mathbf{x}$, we search for the nearest point $\mathbf{x}'$ on the triangle f of mesh, described by barycentric coordinates $\mathbf{w}_b$. For each sampling point, nearest triangle search requires traversing all triangles of mesh, which brings heavy computation. Therefore we accelerate the nearest point search by a CUDA-implemented OCTree. Then we use distance from $\mathbf{x}$ to $\mathbf{x}'$ as distance field value of $\mathbf{x}$, which can be transformed into density value as Eq. (2). Considering our template mesh is non-watertight mesh, we follow Neudf [24] to transform unsigned point-to-mesh-distance into density. Note that there is no noticeable difference in the effects between Neus [38] and Neudf [24].

Normal Approximation. In NeuS [38], SDF normals are obtained via numerical differentiation, enabling calculation at every spatial location, while mesh normals are computed by cross-products of triangle edges and limited to the surface. We address this disparity by approximating the normal $\mathbf{n}$ of sampling point $\mathbf{x}$ using the normal $\mathbf{n}'$ of the nearest point $\mathbf{x}'$. This approximation is accurate when $\mathbf{x}$ is sufficiently close to $\mathbf{x}'$. Its impact on alpha composition of volume rendering is minimal for sampling points far from surface, making the approximation acceptable.

Mesh Sampling. NeuS [38] adopts a coarse-to-fine sampling approach, while assuming objects lie within a sphere and sampling only in this sphere. These two tricks significantly reduce the number of sampling points and accelerate training. We follow the coarse-to-fine sampling strategy but narrow down the sampling range. We compute the first and latest intersection of the rays with the OCTree and sample only within the intersection range, achieving similar results with fewer sampling points. Additionally, NeuS [38] defines a learnable hyperparameter s to automatically control the degree of density distribution concentration. In our experiments, s is set to a fixed value 0.64.

3.3   Mesh Features Spreading

In this section, we introduce our proposed deformation-invariant learnable features spreading module which propagates sparse features defined on mesh surface into the surrounding space to simulate continuous radiance field (as shown in Fig 2). We define implicit feature $A \in \mathbf{R}^{n_a \times n_a \times n_f}$ in UV space to encode the distribution of radiance around surface, where the UV parameterization is predefined by artists. For a sample point $\mathbf{x}$ with its nearest point on mesh (denoted

as $\mathbf{x}'$) described by triangle index and barycentric coordinates $\mathbf{w}_b$, implicit appearance feature $\mathbf{a}' \in \mathbf{R}_{n_a}$ of $\mathbf{x}'$ can be interpolated from A by $\mathbf{w}_b$. Then a MLP $\mathcal{F}_d$ is designed to decode implicit appearance feature $\mathbf{a}'$ with spatial relationship between $\mathbf{x}$ and $\mathbf{x}'$ into color value $\mathbf{c}$ of $\mathbf{x}$, which is trained using shading loss. To model anisotropic radiance, view directions $\mathbf{d}$ are also fed into $\mathcal{F}_d$.

Deformation-invariant Representation. Then the key question is how to represent the spatial relationship between $\mathbf{x}$ and $\mathbf{x}'$. Our features spreading module is designed to propagate features defined on mesh surface into the surrounding space, generating a radiance field. However, since the mesh vertices are also optimized during the reconstruction process, if the surface orientation and position change, the radiance field should also change accordingly to ensure correct rendering after surface changes. Therefore, the spatial relationship between $\mathbf{x}$ and $\mathbf{x}'$ should be defined in the surface's *relative coordinate system* rather than the world coordinate system. In this way, even if the surface orientation and position change, the spatial relationship can remain unchanged.

Relative Coordinate System Transformation. Based on the above observation, we propose an algorithm to calculate surface relative coordinate system and transform sample point $\mathbf{x}$ into the new coordinate system. Given the nearest triangle f of the sample point, the normalized vector from the first edge of the nearest triangle, triangle normal, and the cross product of these two vectors expand a new 3D coordinate system. Each of the three vectors is a unit vector and orthogonal to each other. And we set the nearest point $\mathbf{x}'$ serve as the origin of this relative coordinate system. The new coordinate system expanded by nearest triangle edges and normal can be formulated as:

$$Q = [\mathbf{v_1} - \mathbf{v_0}, (\mathbf{v_1} - \mathbf{v_0}) \times \mathbf{n}, \mathbf{n}], \tag{3}$$

where $\mathbf{v}_i$ is the world coordinate of the i-th vertex of triangle f (represented by column vector), and $\mathbf{n}$ denotes normalized normal.

Then the world coordinates of sample point $\mathbf{x}$ can be transformed into surface relative coordinates $\mathbf{p}_r$ by linear transformation formulated as the following equation:

$$\mathbf{p}_r = Q^{-1}[\mathbf{x} - \mathbf{x}'] \tag{4}$$

View direction $\mathbf{d}$ is transformed into direction $\mathbf{d}_r$ in surface relative coordinate system as $\mathbf{d}_r = Q^{-1}\mathbf{d}$. And finally, the features spreading and radiance prediction process can be formulated as:

$$\mathbf{c} = \mathcal{F}_d(\mathbf{p}_r, \mathbf{d}_r, \mathbf{a}') \tag{5}$$

Additionally, position encoding is involved to increase spatial resolution of $\mathbf{p}_r, \mathbf{d}_r$.

Editing. Due to the relative coordinate transformation, the learned radiance field can move along with the surface, enabling consistent rendering of edited mesh. Similar ray sampling, nearest point search and coordinates transformation are conducted on the deformed mesh.

3.4   Loss and Training Scheme

To reconstruct topology uniformed mesh from multi-view images based on our mesh volume rendering mechanism, we use the following three loss functions to optimize $V, A, \mathcal{F}_d$ for geometry and appearance modeling:

Shading Loss. For geometry and appearance modeling, we use $\mathcal{L}_1$ loss to constrain the shaded images $\hat{I}_i$ computed by mesh volume rendering being close to the real observations I_i:

$$\mathcal{L}_{color} = \sum_i^M |I_i - \hat{I}_i|. \tag{6}$$

Landmark Loss. Landmark loss is involved to constrain the projection of corresponding 3D vertices on mesh are close to 2D detected landmarks for initialization. Noted that 2D landmarks are highly sparse, offering limited shape details, and may involve noise or semantic inconsistency across views, thus landmark loss is only used during the initialization stage. We extract n_l facial landmarks of selected front views denoted by I_f. The landmark loss can be formulated as:

$$\mathcal{L}_{ldmk} = \sum_{\mathcal{I}_f} \sum_{j=0}^{n_l} (p_j^p - p_j^l)^2, \tag{7}$$

where p^p, p^l denote projection and detected landmarks respectively. And the projection process is shown in the following equation, where $K, [R|t]$ denote camera intrinsic and extrinsic parameters for one view:

$$p_j^p = K(Rv_j + t). \tag{8}$$

Mask Loss. The mask loss $\mathcal{L}_{mask}$ is defined as:

$$\mathcal{L}_{mask} = ||M_k - \hat{O}_k||^2, \tag{9}$$

where $\hat{O}_k = \sum_{i=1}^n T_{k,i}\alpha_{k,i}$ is the sum of weights along the camera ray. $M_k \in \{0, 1\}$ is the face mask for the k-th camera view. In practice, mask loss is computed sorely on pixels around the mask contour to reduce sampling rays number and accelerate training. Furthermore, since the UDF volume rendering formula [24] we use cannot distinguish the orientation of mesh, we additionally employ backface culling techniques to set $\hat{O}_k$ of pixels facing away from the camera to zero when calculating the mask loss.

Shape Rigidness. Laplacian regularization [36] is a commonly used shape regularization term in mesh editing. [30] is a neural network compatible Laplacian regularization method with faster and more stable loss reduction. We use it as the shape regularization in our approach for the topology preserving.

Initialization & Iterations. Some initialization methods and iterative training are employed to ensure stable training and convergence speed. Firstly, we use landmark and mask loss to deform the template mesh, initializing geometry. Subsequently the following two steps are iterated until convergence: 1) fix geometry V, while training features spreading module $\mathcal{F}_d$ and appearance A using
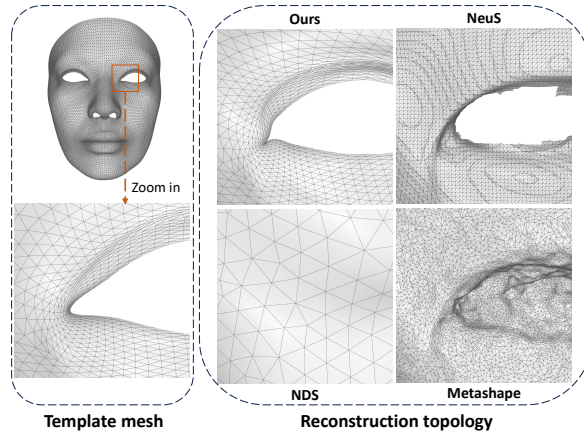
Fig. 3: Illustration of reconstruction topology. The left image shows the topology near the eyes of the template mesh. And the other four images indicate reconstructed mesh topology of four different reconstruction method. It can be observed that our reconstruction results maintains topology consistency with the template mesh and achieve better topology quality.

shading loss; 2) fix $\mathcal{F}_d$ and appearance A, while optimizing V using shading and mask loss.

Training Strategy. When optimizing geometry, due to Laplacian shape rigidness, as one vertex moves the surrounding vertices will also move, so the loss function should be computed using all pixels from multiple views to prevent oscillations. When optimizing $\mathcal{F}_d$ and A, random rays of random images are used to calculate shading loss.

4   Experiments

4.1   Topology & Dataset

We use an Unreal MetaHuman character pre-defined by artists as our template mesh. Following classical 3DMM methods [3,33], we manually segment face region (consisting of 11,763 vertices and 23,004 triangles) from original head mesh and label 106 landmark indices on the region.

Evaluation is performed on multi-view face image dataset released in [40], which includes facial scans of 438 people and 20 expressions for each person. We obtain multi-view images for testing from seven authorized subjects of four identities. For each scan, 30 images are captured with cameras uniformly distributed on a half sphere. The image resolution is $5456 * 3632$, downsampled to $2K$ in our experiments. [40] uses Agisoft's Metashape software to estimate camera parameters and reconstruct facial scans. We additionally implement a non-rigid ICP registration method to deform template mesh to approximate
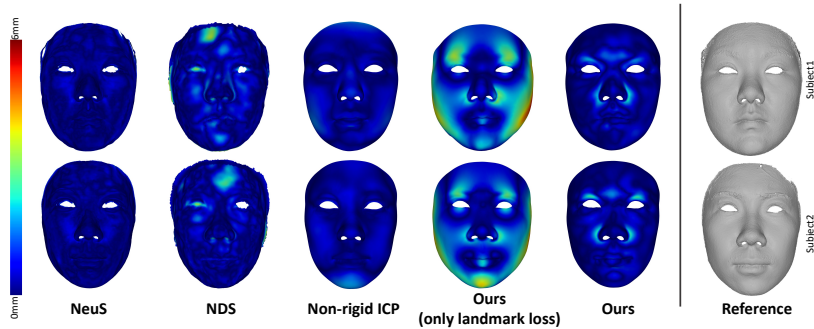
Fig. 4: Comparison of geometry reconstruction of our method with NeuS [38], and NDS [43] using Metashape as reference. We also compare our final reconstruction with registered mesh by non-rigid ICP and mesh constrained by landmark loss only.

scans as comparison. Subsequently, we generate masks using the registration results and estimated camera parameters.

4.2   Implementation details

Our method is implemented in PyTorch and tested on single NVIDIA RTX4090 GPU. In experiments, a four-layer MLP is used as the features spreading module, with 256 hidden layer size and ReLU activation. We set $n_f = 512, n_a = 16$ for implicit texture feature. Adam [16] is used as the optimizer. Learning rate of MLP and implicit feature is set to $8e - 4$ and $5e - 3$ respectively, while learning rate of vertices position is set to $3e - 2$. Laplacian regularization weight of [30] is set to 19. In practice, 32 face contour landmarks are discarded as they are semantically inconsistent across views. For geometry initialization stage, landmark loss and mask loss supervise training for 40 iterations (about 20 minutes). We train $\mathcal{F}_d$ and A with fixed geometry using shading loss for 2000 iterations(about 30 minutes), and then train geometry with fixed appearance parameters for 40 iterations(about one hour). The two steps above are repeated twice.

4.3   Comparisons

We compare the reconstruction accuracy and rendering quality with neural rendering based multi-view reconstruction methods, and compare reconstruction error with MVS with registration procedure. We also demonstrate the rendering effects after face animation. Baseline algorithms are as following: 1) NeuS [38], a widely-used neural volume rendering based reconstruction method. 2) NDS [43], a neural deferred rasterization based multi-view reconstruction method which combines mesh representation and MLP neural shader. 3) Agisoft Metashape, a commercial 3D reconstruction software which performs image feature matching and poisson surface reconstruction to produce high-quality mesh. 4) Metashape
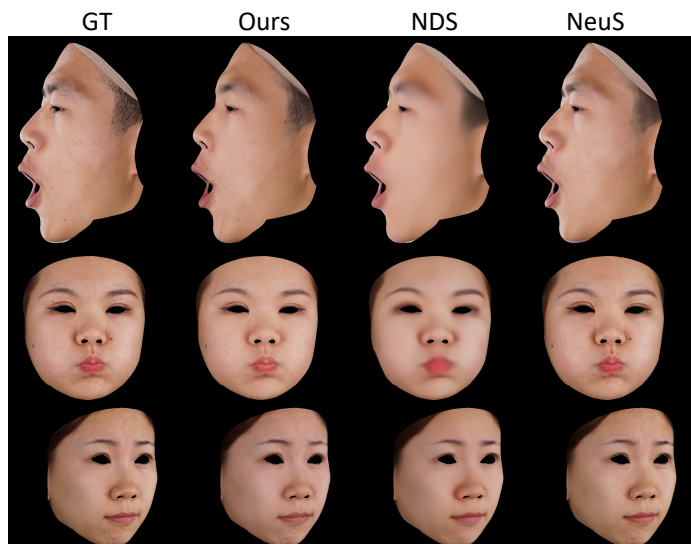
Fig. 5: Comparison of rendering quality to NeuS [38], NDS [43] and ground truth image. Compared to the baselines, our approach can render more facial details. Zoom-in details can be checked in Fig. 6.

with non-rigid registration, classical topology uniformed face mesh reconstruction method. For the sake of fair comparison, we included head masks as input during the training of NeuS [38] and NDS [43]. More results (including ablation study on deformation-invariant feature spreading module) can be found in supplementary materials.

Method	Metashape	NeuS [38]	NDS [43]	Non-rigid ICP	ours($\mathcal{L}_{ldmk}$ only)	ours
Error	-	2.53375	4.71150	3.99536	18.2649	4.08451
Vertex num	110,340	391,508	8,979	11,763	11,763	11,763

Table 1: Reconstruction accuracy comparison with NeuS [38], and NDS [43]. This metric is conducted by computing nearest point-to-mesh distance with Metashape scans. The number of vertices output by Metashape, NeuS [38] and NDS [43] is not fixed. We calculated the average number of vertices for all experimental face meshes.

Geometry Reconstruction. We evaluate the geometry reconstruction qualitatively and quantitatively. We compare our reconstruction with NeuS [38], NDS [43], mesh registration from scans and mesh deformed by $\mathcal{L}_{ldmk}$ only. The minimal distance per vertice between reconstruction and Metashape scan is calculated for quantitative comparison as shown in Table 1 and mapped to color for visualization which can be checked in Figure 4. The hair region of scans
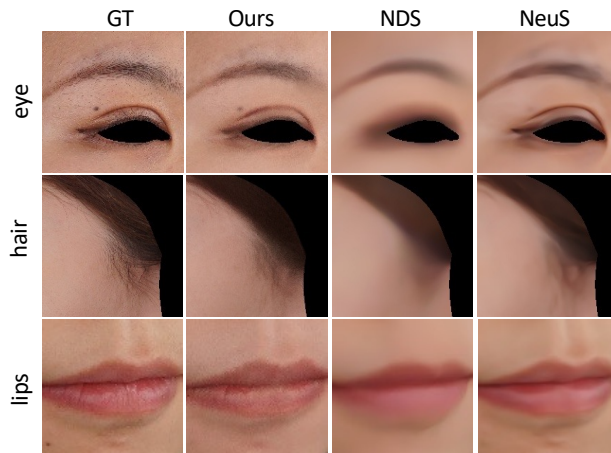
Fig. 6: Face details rendering results.

has relatively high noise, and this part is excluded when calculating distances. Our method achieves better result to NDS [43], and comparable results with non-rigid ICP registration. Note that our reconstructed mesh has notably lower number of vertices compared to NeuS [38] and Metashape, which limits ability of mesh to represent details. Additionally, the non-rigid ICP method aims to closely align with scan, while our objective is to resemble the images. Therefore, using Euclidean distance to Metashape scan as a quantitative metric, the ICP method holds a slight advantage.

Method	PSNR↑	SSIM↑	LPIPS↓
NeuS [38]	27.7589	0.966905	0.358353
NDS [43]	22.5072	0.958411	0.370280
Ours	31.6232	0.993631	0.090816

Table 2: Rendering quantitative comparison with NeuS [38] and NDS [43]. Our rendering results achieve better scores than baseline methods.

Topological Quality of Reconstruction. We also demonstrate the topological quality of the reconstruction results in Figure 3. It can be observed that the mesh topology extracted by Marching Cubes in NeuS has poor quality, while the mesh topology reconstructed by Poisson surface in Metashape is moderate but requires more points to describe the shape. The mesh distribution in NDS is relatively uniform but cannot capture finer details in the eyes. The topology we used is crafted by artists, featuring higher topological quality and allocating more vertices to regions with complex geometry such as eyes and mouth. Our results maintain topology quality and consistency with the template mesh.
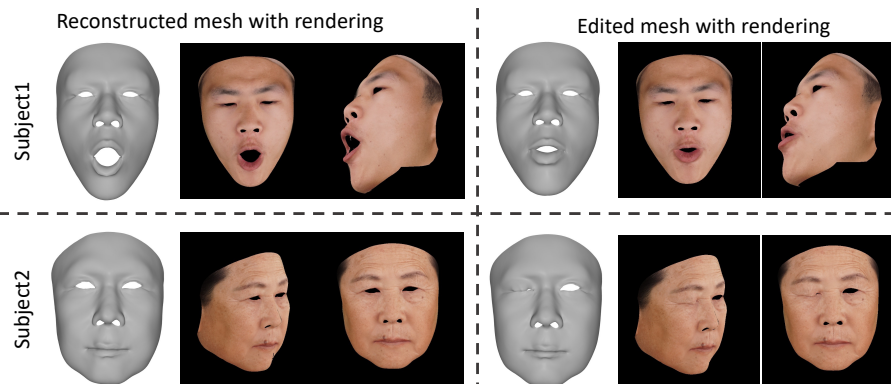
Fig. 7: Mesh editing and rendering. We demonstrate the effectiveness of proposed deformation-invariant feature spreading module by animating the reconstructed mesh and rendering the deformed mesh. Face mesh editing is achieved by blendshapes.

The effects of blendshape animated face shown in Fig 7 also demonstrate the topological consistency.

Rendering quality. Our method has undergone qualitative and quantitative analyses compared with NeuS [38], NDS [43], and the original image. PSNR, SSIM [41], LPIPS [54] are computed to evaluate differences between rendered images with true observations, as shown in Table 2. In qualitative comparisons, Figure 5 reveals that our method achieves better rendering results compared to the baseline methods. Our proposed method performs better than baselines in render facial details such as hair, areas around the eyes, and lip wrinkles, as shown in the zoom-in rendering in Figure 6.

Expression Editing. Our reconstructed mesh can be easily edited using classical mesh deformation methods like blendshapes [18]. After editing, the learned implicit feature and features spreading module can be applied to the deformed mesh seamlessly. Some results are shown in Figure 7.

5 Conclusion

This paper proposes a novel mesh volume rendering mechanism to enable topology-consistent face mesh reconstruction directly from multi-view images. We simulate radiance field by discrete mesh using a deformation-invariant learnable features spreading module to spread sparse surface features into surrounding space. Due to the deformation invariance, the reconstructed geometry and appearance can be rendered seamlessly after editing. Experiments have demonstrate the reconstruction, rendering quality and animated face rendering.

References

1. Bai, Z., Cui, Z., Rahim, J.A., Liu, X., Tan, P.: Deep facial non-rigid multi-view stereo. In: Proceedings of the IEEE/CVF Conference on Computer Vision and Pattern Recognition (CVPR) (June 2020) 4
2. Beeler, T., Hahn, F., Bradley, D., Bickel, B., Beardsley, P.A., Gotsman, C., Sumner, R.W., Gross, M.H.: High-quality passive facial performance capture using anchor frames. ACM Trans. Graph. **30**(4), 75 (2011) 3
3. Blanz, V., Vetter, T., Rockwood, A.: A morphable model for the synthesis of 3d faces. ACM Transactions on Graphics (ToG) pp. 187–194 (2002) 1, 2, 4, 10
4. Bolkart, T., Li, T., Black, M.J.: Instant multi-view head capture through learnable registration. In: Proceedings of the IEEE/CVF Conference on Computer Vision and Pattern Recognition. pp. 768–779 (2023) 2, 4
5. Bolkart, T., Wuhrer, S.: A groupwise multilinear correspondence optimization for 3d faces. In: Proceedings of the IEEE international conference on computer vision. pp. 3604–3612 (2015) 4
6. Cao, C., Simon, T., Kim, J.K., Schwartz, G., Zollhoefer, M., Saito, S.S., Lombardi, S., Wei, S.E., Belko, D., Yu, S.I., et al.: Authentic volumetric avatars from a phone scan. ACM Transactions on Graphics (TOG) **41**(4), 1–19 (2022) 4
7. Chen, W., Litalien, J., Gao, J., Wang, Z., Fuji Tsang, C., Khamis, S., Litany, O., Fidler, S.: Dib-r++: learning to predict lighting and material with a hybrid differentiable renderer. Advances in Neural Information Processing Systems **34**, 22834–22848 (2021) 4
8. Chen, Z., Funkhouser, T., Hedman, P., Tagliasacchi, A.: Mobilenerf: Exploiting the polygon rasterization pipeline for efficient neural field rendering on mobile architectures. In: The Conference on Computer Vision and Pattern Recognition (CVPR) (2023) 2, 4
9. Fyffe, G., Nagano, K., Huynh, L., Saito, S., Busch, J., Jones, A., Li, H., Debevec, P.: Multi-view stereo on consistent face topology. In: Computer Graphics Forum. vol. 36, pp. 295–309. Wiley Online Library (2017) 4
10. Gafni, G., Thies, J., Zollhofer, M., Nießner, M.: Dynamic neural radiance fields for monocular 4d facial avatar reconstruction. In: Proceedings of the IEEE/CVF Conference on Computer Vision and Pattern Recognition. pp. 8649–8658 (2021) 4
11. Ghosh, A., Fyffe, G., Tunwattanapong, B., Busch, J., Yu, X., Debevec, P.: Multi-view face capture using polarized spherical gradient illumination. ACM Transactions on Graphics (TOG) **30**(6), 1–10 (2011) 3
12. Grassal, P.W., Prinzler, M., Leistner, T., Rother, C., Nießner, M., Thies, J.: Neural head avatars from monocular rgb videos. In: Proceedings of the IEEE/CVF Conference on Computer Vision and Pattern Recognition. pp. 18653–18664 (2022) 4
13. Guo, Y.C., Cao, Y.P., Wang, C., He, Y., Shan, Y., Zhang, S.H.: Vmesh: Hybrid volume-mesh representation for efficient view synthesis. In: SIGGRAPH Asia 2023 Conference Papers. pp. 1–11 (2023) 5
14. Hong, Y., Peng, B., Xiao, H., Liu, L., Zhang, J.: Headnerf: A real-time nerf-based parametric head model. In: Proceedings of the IEEE/CVF Conference on Computer Vision and Pattern Recognition. pp. 20374–20384 (2022) 4
15. Jakob, W., Speierer, S., Roussel, N., Vicini, D.: Dr. jit: a just-in-time compiler for differentiable rendering. ACM Transactions on Graphics (TOG) **41**(4), 1–19 (2022) 4

16. Kingma, D.P., Ba, J.: Adam: A method for stochastic optimization. arXiv preprint arXiv:1412.6980 (2014) 11

17. Laine, S., Hellsten, J., Karras, T., Seol, Y., Lehtinen, J., Aila, T.: Modular primitives for high-performance differentiable rendering. ACM Transactions on Graphics **39**(6) (2020) 4

18. Lewis, J.P., Anjyo, K., Rhee, T., Zhang, M., Pighin, F.H., Deng, Z.: Practice and theory of blendshape facial models. Eurographics (State of the Art Reports) **1**(8), 2 (2014) 14

19. Li, T., Bolkart, T., Black, M.J., Li, H., Romero, J.: Learning a model of facial shape and expression from 4d scans. ACM Trans. Graph. **36**(6), 194–1 (2017) 2, 3

20. Li, T., Liu, S., Bolkart, T., Liu, J., Li, H., Zhao, Y.: Topologically consistent multi-view face inference using volumetric sampling. In: Proceedings of the IEEE/CVF Conference on Computer Vision and Pattern Recognition. pp. 3824–3834 (2021) 2, 4

21. Liu, S., Cai, Y., Chen, H., Zhou, Y., Zhao, Y.: Rapid face asset acquisition with recurrent feature alignment. ACM Transactions on Graphics (TOG) **41**(6), 1–17 (2022) 2, 4

22. Liu, S., Li, T., Chen, W., Li, H.: Soft rasterizer: A differentiable renderer for image-based 3d reasoning. In: Proceedings of the IEEE/CVF International Conference on Computer Vision. pp. 7708–7717 (2019) 4

23. Liu, S., Li, T., Chen, W., Li, H.: A general differentiable mesh renderer for image-based 3d reasoning. IEEE Transactions on Pattern Analysis and Machine Intelligence **44**(1), 50–62 (2020) 4

24. Liu, Y.T., Wang, L., Yang, J., Chen, W., Meng, X., Yang, B., Gao, L.: Neudf: Leaning neural unsigned distance fields with volume rendering. In: Proceedings of the IEEE/CVF Conference on Computer Vision and Pattern Recognition. pp. 237–247 (2023) 2, 3, 4, 6, 7, 9

25. Long, X., Lin, C., Liu, L., Liu, Y., Wang, P., Theobalt, C., Komura, T., Wang, W.: Neuraludf: Learning unsigned distance fields for multi-view reconstruction of surfaces with arbitrary topologies. In: Proceedings of the IEEE/CVF Conference on Computer Vision and Pattern Recognition. pp. 20834–20843 (2023) 2, 3, 4, 6

26. Loubet, G., Holzschuch, N., Jakob, W.: Reparameterizing discontinuous integrands for differentiable rendering. ACM Transactions on Graphics (TOG) **38**(6), 1–14 (2019) 4

27. Ma, W.C., Hawkins, T., Peers, P., Chabert, C.F., Weiss, M., Debevec, P.E., et al.: Rapid acquisition of specular and diffuse normal maps from polarized spherical gradient illumination. Rendering Techniques **2007**(9), 10 (2007) 3

28. Meng, X., Chen, W., Yang, B.: Neat: Learning neural implicit surfaces with arbitrary topologies from multi-view images. In: Proceedings of the IEEE/CVF Conference on Computer Vision and Pattern Recognition. pp. 248–258 (2023) 3, 6

29. Mildenhall, B., Srinivasan, P.P., Tancik, M., Barron, J.T., Ramamoorthi, R., Ng, R.: Nerf: Representing scenes as neural radiance fields for view synthesis. Communications of the ACM **65**(1), 99–106 (2021) 2, 4

30. Nicolet, B., Jacobson, A., Jakob, W.: Large steps in inverse rendering of geometry. ACM Transactions on Graphics (TOG) **40**(6), 1–13 (2021) 9, 11

31. Nimier-David, M., Vicini, D., Zeltner, T., Jakob, W.: Mitsuba 2: A retargetable forward and inverse renderer. ACM Transactions on Graphics (TOG) **38**(6), 1–17 (2019) 4

32. Oechsle, M., Peng, S., Geiger, A.: Unisurf: Unifying neural implicit surfaces and radiance fields for multi-view reconstruction. In: Proceedings of the IEEE/CVF International Conference on Computer Vision. pp. 5589–5599 (2021) 4

33. Paysan, P., Knothe, R., Amberg, B., Romdhani, S., Vetter, T.: A 3d face model for pose and illumination invariant face recognition. In: 2009 sixth IEEE international conference on advanced video and signal based surveillance. pp. 296–301. Ieee (2009) 2, 10

34. Peng, Y., Yan, Y., Liu, S., Cheng, Y., Guan, S., Pan, B., Zhai, G., Yang, X.: Cagenerf: Cage-based neural radiance field for generalized 3d deformation and animation. Advances in Neural Information Processing Systems **35**, 31402–31415 (2022) 5

35. Qian, S., Kirschstein, T., Schoneveld, L., Davoli, D., Giebenhain, S., Nießner, M.: Gaussianavatars: Photorealistic head avatars with rigged 3d gaussians. arXiv preprint arXiv:2312.02069 (2023) 4

36. Seidel, H.P.: Laplacian surface editing. In: Proceedings of the 2004 Eurographics/ACM SIGGRAPH symposium on Geometry processing. pp. 175–184 (2004) 9

37. Tang, J., Zhou, H., Chen, X., Hu, T., Ding, E., Wang, J., Zeng, G.: Delicate textured mesh recovery from nerf via adaptive surface refinement. arXiv preprint arXiv:2303.02091 (2023) 4

38. Wang, P., Liu, L., Liu, Y., Theobalt, C., Komura, T., Wang, W.: Neus: Learning neural implicit surfaces by volume rendering for multi-view reconstruction. Advances in Neural Information Processing Systems (2021) 2, 3, 4, 6, 7, 11, 12, 13, 14

39. Wang, X., Guo, Y., Yang, Z., Zhang, J.: Prior-guided multi-view 3d head reconstruction. IEEE Transactions on Multimedia **24**, 4028–4040 (2021) 4

40. Wang, Z., Yu, X., Lu, M., Wang, Q., Qian, C., Xu, F.: Single image portrait relighting via explicit multiple reflectance channel modeling. ACM Transactions on Graphics (ToG) **39**(6) (Nov 2020). https://doi.org/10.1145/3414685.3417824 10

41. Wang, Z., Bovik, A.C., Sheikh, H.R., Simoncelli, E.P.: Image quality assessment: from error visibility to structural similarity. IEEE transactions on image processing **13**(4), 600–612 (2004) 14

42. Wang, Z., Shen, T., Nimier-David, M., Sharp, N., Gao, J., Keller, A., Fidler, S., Müller, T., Gojcic, Z.: Adaptive shells for efficient neural radiance field rendering. ACM Transactions on Graphics (TOG) **42**(6), 1–15 (2023) 2, 5

43. Worchel, M., Diaz, R., Hu, W., Schreer, O., Feldmann, I., Eisert, P.: Multiview mesh reconstruction with neural deferred shading. In: Proceedings of the IEEE/CVF Conference on Computer Vision and Pattern Recognition. pp. 6187–6197 (2022) 4, 11, 12, 13, 14

44. Wu, T., Sun, J.M., Lai, Y.K., Gao, L.: De-nerf: Decoupled neural radiance fields for view-consistent appearance editing and high-frequency environmental relighting. In: ACM SIGGRAPH 2023 conference proceedings. pp. 1–11 (2023) 5

45. Xu, T., Fujita, Y., Matsumoto, E.: Surface-aligned neural radiance fields for controllable 3d human synthesis. In: Proceedings of the IEEE/CVF Conference on Computer Vision and Pattern Recognition. pp. 15883–15892 (2022) 5

46. Xu, T., Harada, T.: Deforming radiance fields with cages. In: European Conference on Computer Vision. pp. 159–175. Springer (2022) 5

47. Yang, B., Bao, C., Zeng, J., Bao, H., Zhang, Y., Cui, Z., Zhang, G.: Neumesh: Learning disentangled neural mesh-based implicit field for geometry and texture editing. In: European Conference on Computer Vision. pp. 597–614. Springer (2022) 5

48. Yang, H., Zhu, H., Wang, Y., Huang, M., Shen, Q., Yang, R., Cao, X.: Facescape: a large-scale high quality 3d face dataset and detailed riggable 3d face prediction. In: Proceedings of the ieee/cvf conference on computer vision and pattern recognition. pp. 601–610 (2020) 2
49. Yariv, L., Gu, J., Kasten, Y., Lipman, Y.: Volume rendering of neural implicit surfaces. Advances in Neural Information Processing Systems **34**, 4805–4815 (2021) 4
50. Yariv, L., Hedman, P., Reiser, C., Verbin, D., Srinivasan, P.P., Szeliski, R., Barron, J.T., Mildenhall, B.: Bakedsdf: Meshing neural sdfs for real-time view synthesis. arXiv preprint arXiv:2302.14859 (2023) 4
51. Yuan, Y.J., Sun, Y.T., Lai, Y.K., Ma, Y., Jia, R., Gao, L.: Nerf-editing: geometry editing of neural radiance fields. In: Proceedings of the IEEE/CVF Conference on Computer Vision and Pattern Recognition. pp. 18353–18364 (2022) 5
52. Yuan, Y.J., Sun, Y.T., Lai, Y.K., Ma, Y., Jia, R., Kobbelt, L., Gao, L.: Interactive nerf geometry editing with shape priors. IEEE Transactions on Pattern Analysis and Machine Intelligence (2023) 5
53. Zhang, C., Smith, W.A., Dessein, A., Pears, N., Dai, H.: Functional faces: Groupwise dense correspondence using functional maps. In: Proceedings of the IEEE Conference on Computer Vision and Pattern Recognition. pp. 5033–5041 (2016) 4
54. Zhang, R., Isola, P., Efros, A.A., Shechtman, E., Wang, O.: The unreasonable effectiveness of deep features as a perceptual metric. In: Proceedings of the IEEE conference on computer vision and pattern recognition. pp. 586–595 (2018) 14
55. Zielonka, W., Bolkart, T., Thies, J.: Instant volumetric head avatars. In: Proceedings of the IEEE/CVF Conference on Computer Vision and Pattern Recognition. pp. 4574–4584 (2023) 4